Fluid Dynamics & Materials Processing FDMP, vol.16, no.1, pp.67-76, 2020

Effect of Streamlined Nose Length on the Aerodynamic Performance of a 800 km/h Evacuated Tube Train

Xiaohan Zhang[1], Yao Jiang[2] and Tian Li[1, *]

Abstract: The aerodynamic resistance of a train running in the open air limits the maximum speed that can be attained by the train. For this reason, evacuated tube trains (ETT) are being considered as valid alternatives to be implemented in the future. The atmosphere in the tube, the so-called blocking ratio and the length of the streamlined nose are the key factors affecting the aerodynamic performances of these trains. In the present work, we investigate evacuated tube trains with different lengths of the streamline nose on the basis of computational fluid dynamics (CFD). The three-dimensional steady compressible Navier-Stokes equations are solved. The running speed of the ETT is 800 km/h and the blocking ratio is 0.2. Results show that with the increase of the streamlined nose length, the aerodynamic drag and lift forces of the head car decrease gradually, and the drag and lift forces of the middle car change slightly. For the tail car, the drag force decreases, whereas the absolute value of the lift force increases. At a speed of 800 km/h, a slight shock wave appears at the rear of the tail car, which affects the aerodynamic forces acting on the train.

Keywords: Evacuated tube train, resistance, aerodynamic performance, streamlined nose.

1 Introduction

The upper speed limit of traditional high-speed trains is affected by dense air near the ground. The air resistance of the running trains will climb with the increase of speed. With the development of science and technology, human being has higher requirements for the speed of ground transportation. Therefore, the study of train aerodynamics is becoming more and more important.

Numerical simulation is a valid tool to study the train aerodynamics. The numerical predictions are compared with experimental measurements at the same Reynolds number to determine the accuracy of each model by Khayrullina et al. [Khayrullina, Blocken, Janssen et al. (2015)]. Three dimensional computations were performed by using the KIVA-3 code to investigate the unsteady compressible turbulent flows around a practical train passing through a single-track tunnel [Ohtsuyama, Yang and Atsushi (1999)]. In order to break through atmosphere restriction and realize the transonic and even supersonic operation of the train, it is necessary to reduce the aerodynamic resistance at a high speed.

[1] State Key Laboratory of Traction Power, Southwest Jiaotong University, Chengdu, 610031, China.

[2] China Railway Eryuan Engineering Group Co., Ltd., Chengdu, 610031, China.

[*] Corresponding Author: Tian Li. Email: litian2008@home.swjtu.edu.cn.

Received: 27 June 2019; Accepted: 14 August 2019.

The aerodynamic resistance and wheel-rail friction resistance are further reduced even eliminated under the low pressure and low density environment and the higher speed of ETT can be achieved. Opgenoord et al. [Opgenoord and Caplan (2018)] studied the aerodynamic issue of the Hyperloop Concept and used an axisymmetric viscous/inviscid coupled boundary-layer method to predict the flow separation and transition.

Similar to the traditional train, there are some similarities for trains running in tunnel and evacuated tube. Pressure waves will generate when the trains are running in the tunnel. A three-dimensional and compressible turbulence model was used to investigate the pressure waves generated while two trains were passing each other in a tunnel by Chu et al. [Chu, Chien, Wang et al. (2014)]. The pressure waves of a high-speed train in a tunnel show complicated variations due to propagation and superposition of the waves [Kim and Rho (2017)]. Some research about the wave phenomena produced by evacuate tube maglev train running at a super high-speed were studied by using 2-D axisymmetric compressible N-S equation [Zhou, Zhang, Li et al. (2019)]. The formation and evolution mechanism of aerodynamic heating in the tube was studied by Niu et al. [Niu, Sui, Yu et al. (2019)]

For the aerodynamic resistances of an evacuated tube train, the relationships between aerodynamic drag force and atmosphere in the tube, the blockage ratio and the running speed were studied by using CFD for a symmetric vehicle [Kim, Kim and Kwon (2011); Liu, Zhang and Zhang (2013); Jia, Wang, Cheng et al. (2018)]. Braun et al. [Braun, Sousa and Pekardan (2017)] designed a kind of Hyperloop pod which can generate lower drag force and effective lift force in the evacuated tube. Airflow characteristics of the vacuum tube transportation with pressure recycle ducts (PRD) and the influence of the interval length and opening width of PRD on the differential pressure were studied [Jia, Wang, Cheng et al. (2018)].

The streamlined nose of the train is closely related to the aerodynamic drag of the train. Therefore, it is particularly important to study the effect of the streamlined nose on the aerodynamic drag of the train. Muñoz-Paniagua et al. [Muñoz-Paniagua and García (2019)]. Zhang et al. [Zhang, Zhang, Li et al. (2018)] studied the aerodynamic optimization of the streamlined nose of the high-speed train under different operating environments. Reducing the aerodynamic resistance of high-speed trains is particularly important for the future high-speed transportation. The streamlined head is an important factor affecting the air resistance. The head shape of a high-speed train was optimized to reduce the resistance based on adjoint method [Zhang, Zhang and Li (2017); Li, Du, Tian et al. (2017)]. The main part of the reduction is the streamlined nose of the train. As known to all, the lower resistance benefits from longer streamlined nose length. However, if it is too long, the trend of resistance will decrease slightly. Therefore, the effect of the streamlined nose length on the aerodynamic performance of ETT is studied at a velocity of 800 km/h.

2 Governing equation

Considering the running environment of the high-speed train in the evacuated tube, it is very important to consider the compressibility of gas when the speed is as high as 800 km/h. The corresponding Mach number is about 0.75 under the condition of 0.2 atm, where the local sound speed is about 295 m/s. The three-dimensional steady compressible Navier-Stokes equation is adopted here, and the governing equation is as follows [Versteeg and

Malalasekera (2007)].

$$\frac{\partial \rho}{\partial t} + div\left(\rho \boldsymbol{u}\right) = 0 \tag{1}$$

$$\frac{\partial \left(\rho u_k\right)}{\partial t} + div\left(\rho u_k \boldsymbol{u}\right) = -\frac{\partial p}{\partial x_k} + div\left(\mu \cdot grad\, u_k\right) + S_M \tag{2}$$

$$\frac{\partial \left(\rho i\right)}{\partial t} + div\left(\rho i \boldsymbol{u}\right) = -p \cdot div\, \boldsymbol{u} + div\left(K\, grad\, T\right) + \Phi + S_i \tag{3}$$

$$p = \rho RT \quad i = C_v T \tag{4}$$

ρ is the air density, t is the time, $\boldsymbol{u}$ is the fluid velocity, u_k is the velocity components in x, y and z directions, μ is the dynamic viscosity, i is the thermodynamic energy, S_M is the momentum source, K is the thermal conductivity, S_i is internal energy, Φ is dissipation function, R is the gas constant, T is temperature and C_v is the mass constant volume heat capacity.

According to the above governing equations, the shear stress transport k-ω model (*SST* k-ω)which provides best of surface pressure among the available Reynold Average Navier-Stokes (RANS) model for passenger train aerodynamics simulations two-equation turbulence model is adopted [Morden, Hemida and Baker (2015)]. And the pressure, temperature and velocity variables in the evacuated tube can be solved by setting reasonable boundary conditions.

3 Computational model

3.1 Train model

A three-unit train model is chosen as the aerodynamic calculation model of the evacuated tube train. It is simplified to be composed of a head car, a middle car and a tail car. The length of the train is 76.2 m, the width is 3.2 m, and the height is 3.6 m. The inter-car gaps of the train are ignored, as shown in Fig. 1. Six different lengths of the streamlined nose are studied, which are 3.5 m, 4.5 m, 5.5 m, 6.5 m, 7.5 m and 10.0 m, respectively.

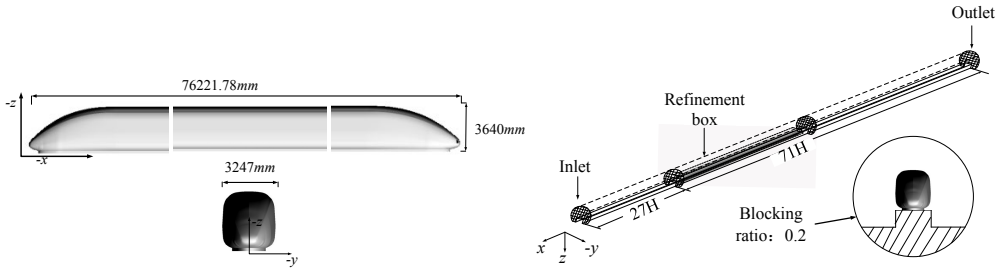

(a) Train model (b) Computational domain

Figure 1: Computational model

The length of the computational domain is 98 H (H represents the characteristic height of the train, which is 3.6 m) and the blocking ratio is 0.2. The distance between the nose tip of the head car and the entrance is 27 H. The nose tip of the tail car is 50 H far from the

exit of the tube. Considering the operation of magnetic levitation, the height between the train bottom and the top surface of the embankment is 20 mm. The width of the embankment is the same as the train.

3.2 Numerical method and boundary conditions

Three-dimensional steady compressible Navier-Stokes equation is adopted in the calculation. The atmosphere in the tube is set as 0.2 atm. When *Kn* (Knudsen number) is less than 0.01, the continuum model can be used to describe the gas flow in this field. [Liu, Zhang and Zhang (2013)]. When the atmosphere is 0.2 atm, $Kn = 3.68 \times 10^{-9}$. Therefore Navier-Stokes equations can be adopted. The incoming velocity of air is 800 km/h. Two-equation *SST k-ω* turbulence model is used. And the kinematic viscosity is satisfied the surtherland condition.

The boundary conditions on the inlet and outlet are set as pressure-far-field which can describe free compressible flow at infinite boundary. The wall without slip is used for the tube and ground.

3.3 Computational mesh

The computational mesh is generated using tetrahedral unstructured grids. The number of grids varies according to the length of the streamlined head, and the total number of elements is in the range of 22 million and 25 million. The height of first boundary layer is 0.04 mm and the number of boundary layer in the height direction is 15. The *y*+ on the train surface is almost less than 3.8. The specific grid is shown in Fig. 2.

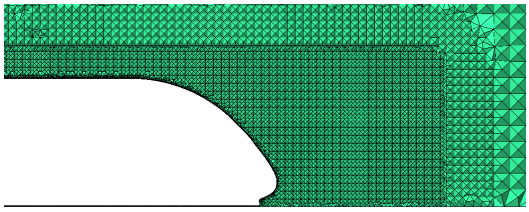

Figure 2: Schematic diagram of the computational mesh

4 Results

The aerodynamic performances of the ETT with different lengths of the streamline nose are numerical simulated using ANSYS Fluent. In the following, the effect of the streamlined nose length on the aerodynamic characteristics is discussed in terms of the aerodynamic performances of the head car, middle car and tail car.

4.1 Head car

Fig. 3 shows the trend of the aerodynamic drag and lift forces of the head car with the increase of the streamlined nose length. The result shows that with the increase of the streamlined nose length, the drag force of the head car will decrease. The drag force are 24.2 kN, when the streamlined nose length is 3.5 m. The drag force can be reduced to 20.5 kN as streamlined nose length increases to 10 m. The reduction of drag is quite obvious.

It can be seen that the lift force of the head car will decrease with the increase of streamlined nose length. When the streamlined nose length changes from 3.5 m to 10 m, the lift force is reduced about 2.8 kN obviously.

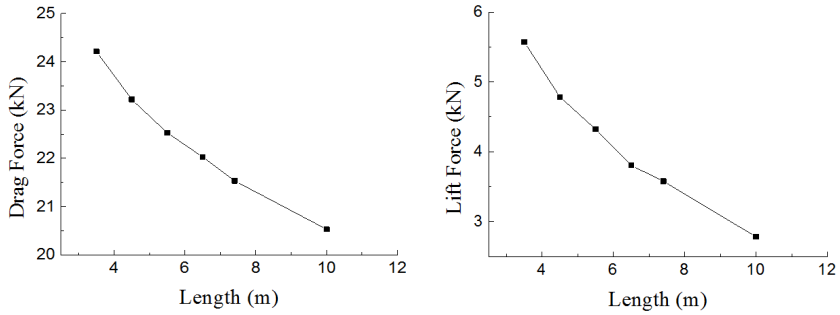

(a) Drag force of the head car (b) Lift force of the head car

Figure 3: Drag and lift forces of the head car with different lengths of the streamlined nose According to the results of drag force above, a fitting curve can be obtained as shown in Formula (5):

$$F = 25.7639 - 0.5488L \tag{5}$$

F is the drag force of head car, L is the length of streamlined nose, 25.7639 and -0.5488 represent intercept and slope of the fitting curve. When the length is 8.6 m, the drag force of head car is predicted as 21.044 kN according to Formula (5).

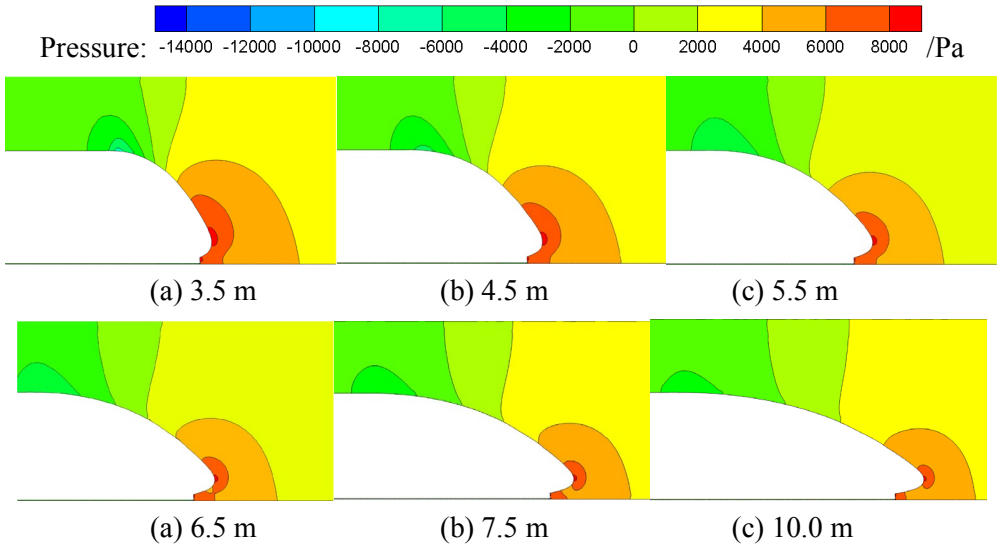

(a) 3.5 m (b) 4.5 m (c) 5.5 m

(a) 6.5 m (b) 7.5 m (c) 10.0 m

Figure 4: Pressure around the head car

The pressure around the head car with different lengths of the streamline nose is shown in Fig. 4. There is a huge positive pressure region at the nose tip. The positive pressure will generate a positive force along the x direction in the streamlined area. With the increase of the streamlined

length, the area affected by the positive pressure at the nose tip will gradually decrease, thus reducing the drag force and downward lift force of the train. At the same time, it will accelerate the flow at the top of the train streamline to form a low pressure zone. When the streamlined nose length is 3.5 m, the negative pressure can reach as low as -6000 Pa to -8000 Pa, as shown in Fig. 4(a). Such low pressure area will cause the upward lift force on the head car. However, it has a relatively small impact on the downward pressure generated at the tip of the head nose. Therefore, the overall lift force is downward.

In order to compare the pressure around the head car, the distribution of pressure along the center line of the streamlined head (x=0 m) is extracted, as shown in Fig. 5. The height of 0 m is the bottom surface of the train body. As shown in Fig. 5, the pressure distribution trend is basically the same at the center line of the car under different streamline types. The pressure reaches its maximum at the nose tip of the train (z=-0.75 m). For all cases, the maximum pressure at the nose tip is about 8533 Pa. With the increase of the streamlined nose length, the positive pressure in the range of z=-0.75 m and -3.0 m decreases significantly, which causes the reduction in the drag and lift forces of the head car.

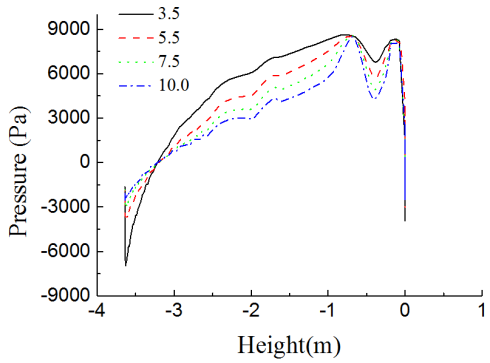

Figure 5: Pressure along the center line of the streamlined nose with different lengths (at a cut plane y=0 m)

4.2 Middle car

Fig. 6 shows the trend of the aerodynamic drag and lift forces of the middle car with the increase of the streamlined nose length. It is found that with the increase of train streamlined nose length, the drag force of mid car will increase slightly with a small magnitude shown in Fig. 6(a). Although the length of streamlined nose increase greatly from 3.5 m to 10.0 m, the drag force has little change about 0.9 kN comparing with the magnitude of change on head car. The lift force is basically unchanged maintaining at around 0.17 kN as shown in Fig. 6(b).

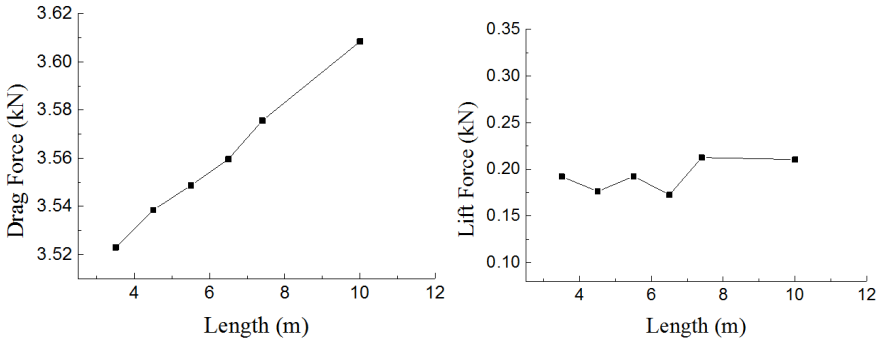

(a) Drag force (b) Lift force

Figure 6: Drag and lift forces of the middle car

As the resistance of the middle car is mainly viscous resistance, the drag and lift forces generated by the middle car have little influence on the whole train.

4.3 Tail car

As can be seen in Fig. 7, the drag force of the tail car decreases with the increase of the streamlined nose length. The magnitude of change on tail car is also great comparing with head car which is reduced about 2.5 kN with the increase of streamlined nose length. And the drag force of tail car change slightly under the lesser streamlined nose length.

The lift force of the tail car is negative, indicating that it is upward. Meanwhile, the lift force almost increases with the increase of the streamlined nose length. When the streamlined nose length increases from 3.5 m to 7.5 m, the value of drag force has more than doubled. Thus it provides that the shock wave affects aerodynamics greatly at the rear of the train. When the increase of streamlined nose length reaches a certain value larger than 7.5 m, the lift force starts increasing slightly.

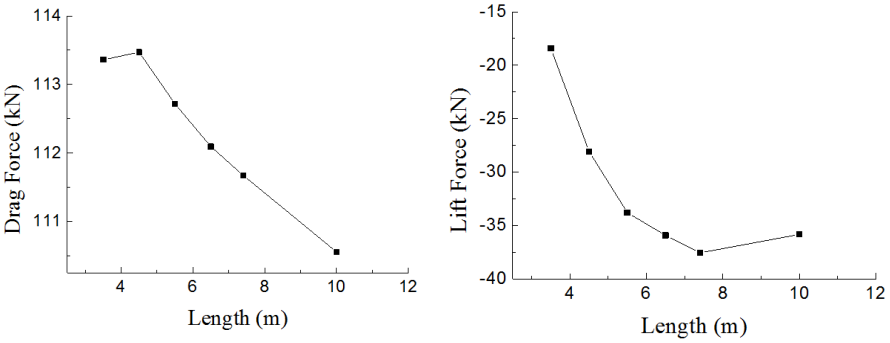

(a) Drag force of tail car (b) Lift force of tail car

Figure 7: Drag and lift forces curves of tail car with different streamlined nose length

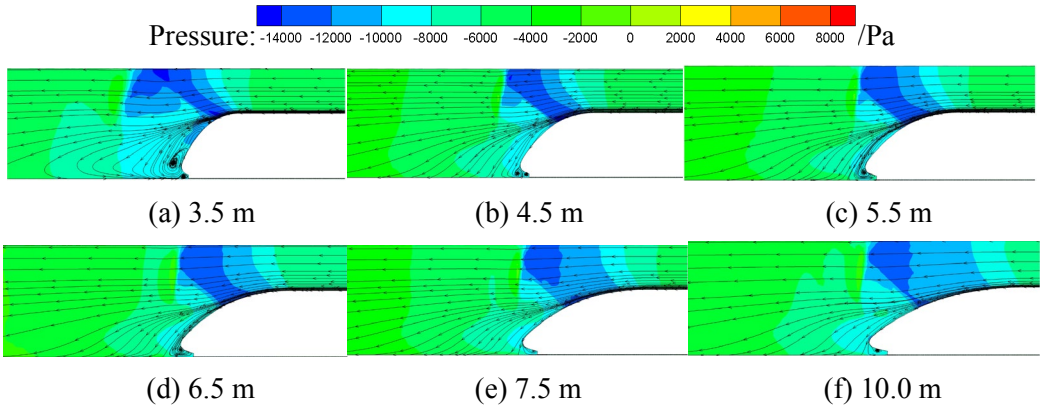

Figure 8: Pressure around the head car with different streamlined nose length

Fig. 8 shows the pressure around the tail car with different streamlined nose length. When the air flow over the tail car, the velocity of airflow will increase and a region with low pressure will generate. Meanwhile, a shock wave will generate due to the extrusion of airflow. It can be seen that when the length of the streamlined nose is 3.5 m, the tail car will generate a vortex, and the low pressure area around the vortex will be larger, which will cause a greater pressure resistance of the tail car. However, the region with low pressure which is about -13000 Pa around the tail car in Fig. 8(a) is smaller than Fig. 8(b). Such distinction leads to the increase in drag force from 3.5 m to 4.5 m shown in Fig. 7(a). With the increase of the streamlined nose length, the region of the very low pressure dissipates slowly. The pressure around the tail car become higher. This changing lead to the decrease of resistance.

The area of low pressure moves slowly from the tail of the train to the top of tail car. Therefore, the lift force of the tail car will become larger. It can be seen in the Fig. 8 that the length of the streamline nose becomes longer and the area of ultra-low pressure becomes smaller, the region of the low pressure will move to the top of the tail car instead of the rear of the tail car. Therefore, it still shows the law of the lift force increases.

5 Conclusion

(1) The aerodynamic drag and lift forces of the head car will decrease with the increase of streamlined nose length.

(2) The streamlined nose has little effect on the aerodynamic drag and lift forces of the mid car. In other words, the aerodynamic forces are less affected by the change of the streamlined nose length, and the drag force increases slightly.

(3) The aerodynamic drag force of tail car decreases with the increase of streamlined nose length. The absolute value of aerodynamic lift force increases with the increase of streamlined nose length, and the trend of change decreases.

(4) When the train speed and the blocking ratio reach certain value, shock waves will occur in the rear area of the train. In the future research, the design of reducing or eliminating the shock wave in the tube train should be paid more attention to.

(5) A longer streamlined nose whose length is less than 10 m is a valid design to reducing the train aerodynamic resistance for ETT.

Acknowledgement: This project was supported by Sichuan Science and Technology Program (No. 2019YJ0227), China Postdoctoral Science Foundation (No. 2019M663550), National Natural Science Foundation of China (No. 51605397) and Science and Technolgoy program of China Railway Group Limited (No. 2018-S-02).

Conflicts of Interest: The authors declare that they have no conflicts of interest to report regarding the present study.

References

Baker, C. J. (2010): The simulation of unsteady aerodynamic crosswind forces on trains. *Journal of Wind Engineering & Industrial Aerodynamics*, vol. 98, no. 2, pp. 88-99.

Adelya, K.; Bert, B.; Wendy, J.; Jochem, S. (2015): CFD simulation of train aerodynamics: train-induced wind conditions at an underground railroad passenger platform. *Journal of Wind Engineering & Industrial Aerodynamics*, vol. 139, pp. 100-110.

Braun, J.; Sousa, J.; Pekardan, C. (2017): Aerodynamic design and analysis of the hyperloop. *AIAA Journal*, vol. 55, no. 12, pp.4053-4060.

Chu, C.; Chien, S.; Wang, C.; Wu, T. (2014): Numerical simulation of two trains intersecting in a tunnel. *Tunnelling and Underground Space Technology*, vol. 42, pp. 161-174.

Cook, P. H.; McDonald, M. A.; Firmin, M. C. P. (1979): Airfoil RAE 2822-pressure distributions and boundary layer and wake measurements. *AGARD Advisory Report*, no.138, pp. A6.

Jia, W.; Wang, K.; Cheng, A.; Kong, X.; Cao, X. et al. (2018): Air flow and differential pressure characteristics in the vacuum tube transportation system based on pressure recycle ducts. *Vacuum*, vol. 150, pp. 58-68.

Kim, J. H.; Rho, J. H. (2017): Pressure wave characteristics of a high-speed train in a tunnel according to the operating conditions. *Proceedings of the Institution of Mechanical Engineers. Proceedings of the Institution of Mechanical Engineers Part F: J Rail and Rapid Transit*, pp.1-8.

Kim, T.; Kim, K.; Kwon, H. (2011): Aerodynamic characteristics of a tube train. *Journal of Wind Engineering & Industrial Aerodynamics*, vol. 99, no. 12, pp. 1187-1196.

Li, G.; Du, J.; Tian, A.; Shang, K. (2017): Aerodynamic optimization of the head shape of a high-speed train based on adjoint method. *2nd International Conference on Industrial Aerodynamics*, pp. 472-480.

Liu, J.; Zhang, J.; Zhang, W. (2013): Analysis of aerodynamic characteristics of high-speed trains in the evacuated tube. *Journal of Mechanical Engineering*, vol. 49, no. 22, pp. 137-143.

Muñoz-Paniagua, J.; García, J. (2019): Aerodynamic surrogate-based optimization of the nose shape of a high-speed train for crosswind and passing-by scenarios. *Journal of Wind Engineering & Industrial Aerodynamics*, vol. 184, pp. 139-152.

Morden, J. A.; Hemida, H.; Baker, C. J. (2015): Comparison of RANS and detached eddy sinulation results to wind-tunnel data for the surface pressures upon a class 43 high-speed train. *ASME Journal of Fluids Engineering*, vol. 137, no. 4, pp. 041108.

Niu, J.; Sui, Y.; Yu, Q.; Cao, X.; Yuan, Y. (2019): Numerical study on the impact of mach number on the coupling effect of aerodynamic heating and aerodynamic pressure caused by tube train. *Journal of Wind Engineering & Industrial Aerodynamics*, vol. 190, pp. 100-111.

Opgenoord, M. M. J.; Caplan, P. C. (2018): Aerodynamic design of the hyperloop concept. *AAIA Journal*, vol. 56, no. 11, pp. 4261-4270.

Sumiaki, O.; Yang, X. F.; Atsushi, O. (1999): Three dimensional CFD analysis of transient compressible flows around a train passing through a tunnel. *Journal of applied mechanics*, vol. 2, no. 1999, pp. 559-566.

Versteeg, H. K.; Malalasekera, W. (2007): *An Introduction to Computation Fluid Dynamics: The Finite Volume Method*. 2nd. Bell &Bain Limited, Glasgow. pp. 21-25

Zhang, L.; Zhang, J.; Li, T.; Zhang, Y. (2018): A multiobjective aerodynamic optimization design of a high-speed train head under crosswinds. *Journal of Zhejiang University-SCIENCE A (Applied Physics & Engineering)*, vol. 18, no. 11, pp. 841-854.

Zhang, L.; Zhang, J.; Li, T. (2017): Aerodynamic optimization of high-speed train head based on adjoint method. *Journal of Mechanical Engineering*, vol. 53, no. 22, pp. 152-159.

Zhou, P.; Zhang, J.; Li, T.; Zhang, W. (2019): Numerical study on wave phenomena produced by the super high-speed evacuated tube maglev train. *Journal of Wind Engineering & Industrial Aerodynamics*, vol. 190, pp. 161-170.